HHS Public Access

Author manuscript

Cell Rep. Author manuscript; available in PMC 2019 September 21.

Published in final edited form as:

Cell Rep. 2019 March 12; 26(11): 2859–2867.e4. doi:10.1016/j.celrep.2019.02.034.

Interstitial migration of CD8αβ T cells in the small intestine is dynamic and is dictated by environmental cues

Emily A. Thompson[1,2], **Jason S. Mitchell**[2,3], **Lalit K. Beura**[1,2], **David Torres**[5], **Paulus Mrass**[6], **Mark J. Pierson**[2,3], **Judy L. Cannon**[6], **David Masopust**[1,2], **Brian T. Fife**[2,4], **Vaiva Vezys**[1,2,*]

[1]Department of Microbiology and Immunology, University of Minnesota, Minneapolis, MN 55455

[2]Center for Immunology, University of Minnesota, Minneapolis, MN 55455

[3]Department of Laboratory Medicine and Pathology, University of Minnesota, Minneapolis, MN 55455

[4]Department of Medicine, University of Minnesota, Minneapolis, MN 55455

[5]Department of Mathematics and Physical Science, Northern New Mexico College, Espanola, NM 87532

[6]Department of Molecular Genetics and Microbiology, University of New Mexico, Albuquerque, NM 87131

Summary

The migratory capacity of adaptive CD8αβ T cells dictates their ability to locate target cells and exert cytotoxicity, which is the basis of immune-surveillance for containment of microbes and disease. The small intestine (SI) is the largest mucosal surface and is a primary site of pathogen entrance. Using two-photon laser scanning microscopy, we found that motility of antigen (Ag)-specific CD8αβ T cells in the SI is dynamic and varies with the environmental milieu. Pathogen-specific CD8αβ T cell movement differed throughout infection, becoming locally confined at memory. Motility was not dependent on CD103 but was influenced by micro-anatomical locations within the SI and by inflammation. CD8 T cells responding to self-protein were initially affected by the presence of self-Ag, but this was altered after complete tolerance induction. These studies identify multiple factors that impact CD8αβ T cell movement in the intestinal mucosa and show the adaptability of CD8αβ T cell motility.

Introduction

The small intestine (SI) is the largest mucosal interface between the host and the outside environment and is the entry site for many microbes, which can quickly disseminate

*Corresponding author and lead contact Vaiva Vezys, Ph.D., University of Minnesota, Center for Immunology, 2-180 Wallin Medical Biosciences Building, 2101 6th St SE, Minneapolis, MN 55455, vvezys@umn.edu, Tel: 612-625-4650, Fax: 612-625-2199.

Author contributions

E.A.T., J.S.M, L.K.B, and M.J.P performed experiments and analyzed the data. P.M., D.T. and J.L.C. calculated parameters of motility and performed modeling experiments. E.A.T., L.K.B., B.T.F., D.M., and V.V. designed experiments. E.A.T. and V.V. wrote the manuscript.

Declaration of interests

The authors declare no competing interests.

throughout the body. Therefore, evaluating immune cell surveillance in this compartment is of great interest. Many elegant studies have assessed the motility of unconventional and CD4 T cells in the SI, but the migratory behavior of adaptive CD8αβ T cells in this tissue is unknown (Edelblum et al., 2012; Hoytema van Konijnenburg et al., 2017; Sujino et al., 2016; Sumida et al., 2017; Wang et al., 2014; Xu et al., 2012). After systemic lymphocytic choriomeningitis virus (LCMV) infection that broadly positions CD8 T cells throughout the mouse, there are only six Ag-specific CD8 resident memory T cells (T_{RM}) found per every 1000 nucleated cells in the SI at a memory time point (Steinert et al., 2015). This, combined with the distinctive sub-anatomical features of the SI, creates a unique challenge for adequate patrolling of this tissue by CD8 T cells.

Using two-photon laser scanning microscopy (TPLSM), we show that CD8 T cell motility in the SI jejunum is dynamic and largely dependent on context, such as the stage of infection and inflammatory milieu. Furthermore, the physical location of CD8 T cells within anatomical compartments of the SI dictated their migratory behavior. Dissecting the motile behavior of CD8 T cells during the steady state and infection has broadened our knowledge of effective CD8 T cell immune-surveillance in the SI and informs the development of vaccines and treatments targeting pathogens or malignancies requiring CD8 T cell responses.

Results

Ag-specific CD8αβ T cell motility in the small intestine is dynamic during infection

To assess the motile behavior of CD8 T cells during infection, naïve P14-GFP CD8 T cells, which recognize the gp33 epitope of LCMV, were transferred to B6 mice that were subsequently infected with LCMV (Figure S1A). At days 5, 8 and 30 after LCMV infection, P14-GFP CD8 T cells were detected in both the epithelium and lamina propria (LP) of the SI using flow cytometry (Figure S1B). At all time points, P14-GFP CD8 T cells in the villi of explanted jejunum were motile in three dimensions (Figures 1A and S1C, Movies S1–2). While P14-GFP CD8 intraepithelial lymphocytes (IEL) continuously probed the tissue, P14-GFP CD8 LP lymphocytes (LPL) exhibited a smooth, gliding motion along other cells (Movies S1–2). Interestingly, we observed P14 CD8 T cells moving between the epithelium and the lamina propria, which has been seen with γδ T cells (Sujino et al., 2016). Antigen-specific P14-GFP CD8 T cells were never observed “space walking”-i.e., traversing the lumen between villi. Occasionally, CD8 T cells traveled from villus to villus through the LP at the base of the villi near crypt-villi junctions (data not shown). Villi tilting during imaging was common and made quantification of cell movement between the epithelium and LP difficult, as well as delineating motility of T cells confined to those areas. Day 5 effector P14-GFP CD8 T cells moved at ~5μm/minute and, by day 8, their speed increased nearly 1.5-fold (Figures 1B and S1D, Movie S1). Effector T cells are large to keep up with cellular demands early after infection (4–8 days). We saw that T cells were most highly motile at day 8 following infection, even though they were quite large, indicating cell size did not hinder T cell locomotion. At memory, when most CD8 T cells become T_{RM}, their speed was significantly slower than day 8 (Figures 1B and S1D, Movies S1–2). The migration of

effector CD8 T cells was also assessed in an intact anesthetized mouse using an OT-I-GFP/VSV-OVA infection model and similar behaviors were observed (Movie S3).

Normalizing T cell tracks to the same point of origin showed that early (day 5) and peak (day 8) effector CD8 T cell tracks were not constrained in any direction; however, T_{RM} were restrained (Figure 1C). This was further verified by a greater median turning angle and lower confinement ratio of T_{RM} compared to effector T cells (Figures 1D–E and S1E–F). The turning angle measures the angle at which a cell deviates from its direction of travel. A high turning angle indicates a cell is turning sharply while a lower turning angle indicates the cell is continuing in a similar direction of travel (less restricted). Confinement ratio measures the displacement of the cell divided by its path length. Displacement is a measurement of the shortest distance between an initial point to the final position. Therefore, cells with more restricted motility have a lower confinement ratio, as this indicates minimal displacement over a longer path length (Cahalan and Parker, 2008; Germain et al., 2012). We also assessed the "straightness" of cell tracks using a previously described *Z*-score metric which determines whether experimental displacement is less than ("confined tracks") or higher than ("straight tracks") what is expected by chance (Mrass et al., 2017). T_{RM} tracks had the lowest *Z*-score of any time point measured, suggesting memory T cell motility is more constrained than effector P14 CD8 T cells (Figure 1F). Accordingly, memory T cells also scanned a significantly lower volume than did effector CD8 T cells in the SI and did not exhibit directed migration, as determined by mean squared displacement (MSD) (Figure 1G–H). Taken together, these results suggest that, in contrast to effector CD8 T cells, memory CD8 T cells display markedly confined motility.

T_{RM} migration in the small intestine is locally restricted and independent of CD103

Our imaging analysis showed that memory CD8 T cells scanned a smaller volume of tissue compared to effector CD8 T cells, which suggested that this may impact the efficiency of immune-surveillance in this tissue (Figure 1). To understand the surveillance requirement in a villus, we performed mathematical modeling based on our various assessed parameters for T_{RM} movement. Our model estimated that it would take nearly 28 hours for 60 CD8 T_{RM} to completely scan a single villus and approximately a month for a single T_{RM} to do the same (Figures 2A and S2A). However, our experiments could not distinguish whether CD8 T cell populations are fixed in a particular location of the SI over time or whether there is migration of T cells between areas. To test this, we used the Kaede reporter mouse, that allows tracking of cells after *in vivo* labelling through photoconversion (Tomura et al., 2008). The establishment of OT-I/Kaede T_{RM} was confirmed via parabiosis (Figure S2B). A piece of the ileum of OT-I/Kaede memory mice was surgically exteriorized and exposed to a 405nm light for photoconversion and the position of converted T cells was assessed after 1 or 7 days (Figures 2B and S2C). Photoconverted OT-I/Kaede IEL and LPL (Kaede-red) were present in the ileum of mice exposed to violet light, but remained undetectable in sham surgery controls. Very few (<1%) of converted OT-I/Kaede CD8 T cells were detected in the jejunum, duodenum, spleen or mesenteric lymph node (MLN) and no significant differences in frequency of converted cells were observed between 24 hours and 7 days (Figures 2C–D and S2D). These data indicate that memory CD8 T cells in the SI are limited to surveying relatively narrow areas. In a separate experiment, TPLSM was performed on the ileum of

OT-I/Kaede mice before and after conversion verifying that light exposure did not impact T cell motility (data not shown).

We next wondered what was responsible for the confined motility of T_{RM} in the SI. In both the skin and liver, CD8 T cell interactions with integrins have been shown to be important for T cell behavior (McNamara et al., 2017; Overstreet et al., 2013; Santamaria Babi et al., 1995). We speculated that CD103 interaction with E-cadherin might be responsible, as this is crucial for T_{RM} maintenance in the epithelium of the SI and heightened expression of CD103 (along with CD69) upon memory formation correlated with restricted motility (Figures S3A–B) (Casey et al., 2012). Surprisingly, no changes in motility were observed between CD103 sufficient and deficient P14 CD8 T cells at any time point (days 8, 14, 30) evaluated (Figures 2E–G and S3C–F, Movie S4). It was difficult to assess whether the absence of CD103 impacted intraepithelial migration and probing, as Hoechst dye could not be used due to spectral overlap and second harmonic generation (SHG) does not clearly distinguish between the lamina propria and epithelium. Similar results were observed with experiments using RGD peptides to block interactions between integrins and several components of the extracellular matrix (ECM) (data not shown). These results suggest that integrins do not contribute to T_{RM} locomotion.

Small intestine tissue architecture dictates CD8 T cell motility

Tissue composition can affect CD8 T cell motility (Germain et al., 2012; Overstreet et al., 2013; Sorokin, 2010). We inquired whether the complex and unique tissue architecture of the SI could impact CD8 T cell interstitial migration. The SI can be divided into 4 unique layers: serosa, muscularis externa, submucosa and mucosa (Figure 3A) (Mowat and Agace, 2014; Wright et al., 1989). In the serosa and longitudinal muscle, P14-GFP CD8 T cells were elongated parallel to myocytes, while T cells in the less dense circular muscle maintained an amoeboid shape (Figures 3B–C, Movies S5–6). At both days 5 and 8, P14-GFP CD8 T cells in the muscularis externa had shorter path lengths and were slower and more confined, as compared to CD8 T cells in the crypts (Figures 3D–H, Movies S5–6). The volume scanned by P14-GFP CD8 T cells increased between day 5 and day 8 in both the serosa and the crypt, without a change in confinement measurements (Figure 3I). Remarkably, CD8 T cells in the crypt often orbited around its entire planar section. Alternatively, effector CD8 T cells in the serosa exhibited low *Z*-scores, indicating confined motile behavior (Figure 3J). T_{RM} were nearly completely absent from the serosa and crypt, which suggests that P14 T cells are excluded from those compartments after LCMV infection subsides. Taken together, these results indicate that Ag-specific CD8 T cells in the SI rely on the immediate tissue architecture to influence their migratory pattern.

Inflammation alters T_{RM} patrolling behavior

Reports indicate inflammation can cause alterations to tissue architecture that can affect T cell migration (Hallmann et al., 2015; Mueller, Hosiawa-Meagher, et al., 2007; Mueller, Matloubian, et al., 2007; Zaid et al., 2014). Since we observed striking differences in motility based on the location of CD8 T cells within the SI, we wondered whether bystander inflammation could drive changes in T_{RM} motility, possibly due to reorganization of the ECM. P14-GFP CD8 T cell memory mice received naive OT-I-CFP CD8 T cells and were

orally infected with *Yersinia pseudotuberculosis* expressing ovalbumin (Yptb-OVA) (Figure 4A) (Bergsbaken and Bevan, 2015). At day 6 following Yptb-OVA infection, the speed of P14-GFP CD8 T_{RM} was not altered by bystander inflammation; however, these T cells were less constrained as compared to the steady state: their turning angle was significantly decreased and the confinement ratio was slightly increased (Figures 4B–D, S4A–C, Movie S8). Effector OT-I-CFP T cells exhibited a migration pattern comparable to effector P14-GFP CD8 T cells following LCMV (Figures 4B–D, Movie S8). While bystander inflammation has some impact on memory T cell motility, T_{RM} do not match the motility of effector T cells in the very same inflammatory environment, suggesting some behaviors are antigen driven or cell intrinsic. We next tested the impact of acute inflammation on P14-GFP CD8 T_{RM} behavior using LPS-induced endotoxemia. Interestingly, T_{RM} became more restricted in comparison to steady state conditions, having a wider turning angle (Figures 4E–G, S4D–F, Movie S9). These results show that the motility of T_{RM} in response to various types of inflammation is dynamic.

As the SI is a portal of microbial entry, it needs to maintain active immune surveillance; however, it must also curtail inappropriate immune responses to self-protein, normal flora and food antigen (Konjar et al., 2017). We next addressed whether the motility of self-specific CD8 T cells would be impacted by the presence of auto-antigen in the SI. We used mice which produce ovalbumin under the control of the intestinal fatty acid binding protein promoter (iFABP-OVA) which limits OVA expression to mature enterocytes of the SI (Vezys et al., 2000). Five days after transfer, tolerant OT-I cells were detected in the lamina propria and the epithelium in large numbers and displayed slowed migration speed (~4μm/minute) with frequent arrests (Figures 4H and S4G–L) (Pauken et al., 2015). Arrest was due to the presence of Ag, as blocking K^b-SIINFEKL complexes resulted in significantly increased mean track speed (Figure 4H, Movie S10). However, this did not impact other measurements of motility (Figures 4I–J, S4L, Movie S10). At day 10 following transfer, when tolerance is more established, OT-I-GFP CD8 T cells migrated at a two-fold higher speed in comparison to day 5 OT-I-GFP CD8 T cells and were not impacted when interactions with antigen were blocked (Figures S4G–O). These data indicate that, as T cells fully differentiate to a tolerant state, they become incapable of antigenic interaction, which impacts their motility.

Discussion

The expansive and ever-changing milieu of the gut likely necessitates plastic and adaptable T cell motility to achieve effective immune-surveillance of this compartment. The constant balance between activation and suppression makes the SI perhaps the most dynamic immune environment in the host (Chistiakov et al., 2015; Cieza et al., 2012). We found that Ag-specific CD8 T cell motility in the SI varied greatly depending on the presence of Ag, the inflammatory context and the surrounding tissue architecture. Initial arrest of T cells at early time points after infection was likely due to TCR engagement with Ag, signaling the cell to slow down (Figures 1, S1) (Celli et al., 2011; Dustin et al., 1997). The increase in speed at day 8 may be to optimize T cell scanning once local Ag is cleared, as the volume scanned by P14 CD8 T cells was greatest at this time point in the crypts and villi (Müller et al., 2000). Similar observations have been made in many solid tumor models (Boissonnas et al., 2007; Breart et al., 2008; Mrass et al., 2006).

In contrast, CD8 T_{RM} were highly confined, even given the need to survey such an expansive environment (Figures 1, S1). This was not observed in T_{RM} found in the female reproductive tract or liver, where T cells are highly motile (Beura et al., 2018; Fernandez-Ruiz et al., 2016). While we suspected that the CD103 integrin may be responsible for this restricted T cell behavior at memory time points in the SI, the loss of CD103 in P14 CD8 T cells had surprisingly no impact on T cell locomotion (Figures 2E–G, S3C–F). It is likely that the architecture of the SI supersedes targeted motility, e.g. the most direct route from one point to another may be by "space walking" across the intestinal lumen, which we did not observe. To this point, CD8 T cells were confined to orbiting crypts and circling within villi. Additionally, results from mean squared displacement indicated that cells in the villi were not directed and exhibited more of a Brownian motion (Figure 1H). As CD8 T cell motility in the SI was not mediated by integrins, we wondered if confinement was due to reorganization of the ECM after infection subsides. This could be similar to effector CD8 T cells in the muscularis layer of the SI, which were seemingly held between muscle cells and potentially confined because of this (Figure 3). Throughout the course of infection, the ECM can be considerably reorganized and differences in tissue architecture can impact T cell motility (Overstreet et al., 2013; Sorokin, 2010). Indeed, at day 14 after LCMV infection, T cells exhibited motility that was midway between days 8 and day 30 (Figures S1D–F). Interestingly, during an antigenically distinct local infection with Yptb-OVA or introduction of LPS, T_{RM} motility was disparately impacted (Figures 4, S4A–F). This indicates that CD8 T cells adapt their migratory behavior depending on various inflammatory cues. Effector T cells in the same environment displayed distinct locomotion, as compared to bystander memory T cells, validating that certain behaviors are antigen driven and/or are intrinsic to effector T cells. At day 5, self-specific CD8 T cells were slightly more confined and slower than P14 CD8 T cells at effector time points (Figures 1, 4H–J). This enforces the concept that the less hindered mobility of effector T cells could be due to microbial induced inflammation and tissue restructuring, as OT-I transfer to iFABP-OVA mice does not induce high levels of inflammation (Vezys et al., 2000).

Our studies demonstrate that CD8 T cell mobility in the SI is disparate throughout the course of infection and may be governed by the complex tissue architecture of the SI. Surprisingly, interactions with integrins do not impact CD8 T cell motility, but T_{RM} locomotion is influenced by the local inflammatory milieu. This work informs the requirements for therapies dependent on efficient CD8 T cell immune-surveillance of the SI and suggests that, given their restricted motile behavior, large numbers of CD8 T_{RM} in the SI are required for effective immunity against microbes and malignancies.

STAR METHODS

CONTACT FOR REAGENT AND RESOURCE SHARING

Further information and requests for resources and reagents should be directed to and will be fulfilled by the Lead Contact, Vaiva Vezys (vvezys@umn.edu).

EXPERIMENTAL MODEL AND SUBJECT DETAILS

C57BL/6J (B6), C57BL/6-Tg (UBC-GFP)30Scha/J (ubiquitin-GFP), Tg(CAG-ECFP)CK6Nagy/J (actin-ECFP), B6.129S2(C)-*Itgae*^{tm1Cmp}/J (CD103KO), B6.Cg-Tg(Itgax-Venus)1Mnz/J, and B6 Thy1.1 mice were purchased from The Jackson Laboratory. B6 CD45.1 mice were purchased from Charles River Laboratories. All mice were maintained in specific pathogen free conditions at the University of Minnesota. iFABP-OVA, P14/CD45.1, and OT-I/CD45.1 mice were bred and maintained in house. Kaede mice were a generous gift from Dr. Kristin Hogquist (University of Minnesota). P14 and OT-I reporter mice were generated by crossing the TCR Tg mice with ubiquitin-GFP or actin-ECFP mice. P14-CFP^{+} CD103$^{-/-}$ mice were generated by crossing P14-CFP^{+} mice to P14^{+} CD103$^{-/-}$ mice. Kaede B6 mice were crossed to OT-I mice to generate OT-I/Kaede reporter mice (Tomura et al., 2008). Adult male and female adult mice ranging from 10–32 weeks of age were used in experiments. All mice were housed under standard conditions in animal facilities and used in accordance with the Institutional Animal Care and Use Committees guidelines at the University of Minnesota.

METHOD DETAILS

Infections—P14 immune chimeras were generated by transferring 5×10^4 P14-GFP CD8 T cells into naïve B6 mice intravenously (i.v.) followed by infection with 2×10^5 plaque-forming units (PFU) LCMV Armstrong via intraperitoneal (i.p.) injection one day later. For CD103−/− experiments, 2.5×10^4 P14-GFP CD8 T cells and 2.5×10^4 P14-CFP CD8 CD103−/− T cells were co-transferred to naïve B6 mice i.v. and infected with LCMV-Armstrong i.p. one day later. For OT-I and OT-I/Kaede immune chimeras, 5×10^5 naïve OT-I Kaede cells were adoptively transferred to B6 mice i.v. One day later, mice were infected with 1×10^6 PFU of VSV- OVA i.v.

For experiments evaluating the impact of bystander inflammation on memory CD8 T cell responses, 5×10^4 P14-GFP CD8 T cells were transferred into B6 mice, which were infected the next day with LCMV. At least 30 days later, these same mice received 5×10^5 naïve OT-I-GFP CD8 T cells i.v. and were infected orally with 1×10^8 Yptb-OVA CFU (provided by Dr. Tessa Bergsbaken, Rutgers University) 1 day later (Bergsbaken et al., 2017). For experiments with LPS, 4mg/kg of LPS was i.p. injected into P14-GFP memory mice. 4–5 hours after injection, tissue was harvested for imaging. In studies evaluating self-specific responses, 5×10^5 naïve OT-I-GFP CD8 T cells were transferred to iFABP-OVA mice. iFABP-OVA mice were not exposed to any infectious agents.

Parabiotic surgery—Parabiotic surgery was performed as previously described (Schenkel et al., 2013). Briefly, each mouse to be paired was shaved along the opposite lateral flank. The skin was sterilized and an incision was made on the lateral aspect of each mouse. The lateral skin incisions were conjoined using surgical wound clips. Parabionts were rested for 14–30 days before experiments. Equilibration was confirmed in the peripheral blood prior to the experimental endpoint.

Photoconversion of OT-I/Kaede CD8 T cells—Mice were anesthetized with i.p. injection of Avertin (2,2,2-Tribromalethanol) (250mg/kg). The upper abdominal area of the

anesthetized mice was shaved and cleaned with Povidone iodine solution followed by 70% alcohol and a 1–2cm long, horizontal midline incision was made to expose the peritoneum. The intestine was visualized by gently retracting the skin and then a second 1–1.5cm incision was made to open the peritoneal cavity. A small loop (1cm^2) of the ileum was carefully pulled through the opening in the peritoneal cavity. Three separate spots in the tissue (~2mm^2) were exposed to a 405nm violet light at 100mW/cm^2 power for 3min/spot. The loop of intestine was returned to the peritoneal cavity and the peritoneal wall was closed with monofilament synthetic absorbable surgical suture. The skin was closed with 3–4 wound clips. Extreme care was taken to avoid activating Peyer's patches and mesenteric lymph nodes. Tissue was harvested 1 or 7 days post conversion.

Tissue harvesting and processing—Organs were harvested and digested as previously described (Thompson et al., 2016). For isolation of SI IEL, Peyer's patches were removed, the SI was cut longitudinally and then laterally into small pieces. Pieces were incubated for 30 minutes with stirring at 37°C with 0.154mg/mL dithioerythritol (Sigma-Aldrich, St. Louis, MO) in 10% HBSS/HEPES. The pieces were vortexed on high speed to dislodge intraepithelial lymphocytes and the supernatant was collected. The SI pieces were washed in RPMI containing 5% FBS and put in RPMI 1640 containing 5% FBS, 2 mM $MgCl_2$, 2 mM $CaCl_2$ and 0.5mg/mL 100 U/mL type I collagenase (Worthington, Lakewood, NJ) and incubated for 45 minutes at 37°C with stirring to obtain LPL. After enzymatic digestion, the remaining tissue pieces were mechanically disrupted using a gentleMACs dissociator (Miltenyi Biotec, San Diego, CA). Single cell suspensions from supernatant of the digestions were further separated using a 44%/67% Percoll (GE Healthcare Life Sciences, Pittsburgh, PA) density gradient. Spleen and lymph nodes (LN) were dissociated mechanically. Splenocytes and blood were treated with ACK lysis buffer to lyse red blood cells.

Tissue freezing, immunofluorescence and microscopy—Harvested murine tissues were fixed in 2% paraformaldehyde for 2 hrs before being treated with 30% sucrose overnight for cryoprotection. Sucrose treated tissue was embedded in tissue freezing medium OCT and frozen in an isopentane liquid bath. Frozen blocks were processed, stained, and imaged. Stains included antibodies targeting the following markers: E-cadherin (DECMA-1, Abcam), collagen IV polyclonal antibody (Millipore), CD31 (MEC13.3, BD Horizon, San Jose, CA). Bovine α-goat (polyclonal) was used as a secondary antibody (Jackson Immunoresearch, West Grove, PA).

Flow cytometry and peptide stimulation—Isolated lymphocytes were surface or intracellular stained with antibodies indicated in the Key Resources table. Peptide stimulation was performed as previously described (Beura et al., 2015). Briefly, lymphocytes were plated in RPMI 1640 containing 10% FBS, 1x NEAA, 2mM L-glutamine, 1mM sodium pyruvate, 1x penicillin/streptomycin and 0.05mM β-mercaptoethanol and incubated with 1μg/mL SIINFEKL peptide for four hours at 37°C. All samples also contained1μg/mL GolgiPlug (BD Biosciences, San Jose, CA). Cells were washed and stained with surface and intracellular antibodies. For intracellular stains, the BD Biosciences intracellular kit for cytokine staining was used in accordance with manufacturer's instructions. Ghost Dye™

Red 780 (Tonbo Biosciences, San Diego, CA) was used during surface staining to evaluate cell viability. Stained samples were acquired using LSRII or LSR Fortessa flow cytometers (BD Biosciences) and analyzed with FlowJo software (Treestar).

Two-photon laser scanning microscopy and analysis

Microscopy procedure: A piece of apical jejunum was harvested into warm RPMI 1640 containing 5% FBS, cut longitudinally, and mounted on a cover slip. For experiments with Hoechst stain (Invitrogen), mice were injected i.v. with 1mg of Hoechst stain 30 minutes to 24 hours before imaging. For intravital experiments, mice were anesthetized with 2–5% isoflurane continuously inhaled delivered via nose cone. The mouse abdomen was scrubbed with 70% ethanol and a 1–2cm horizontal midline incision was made to expose the peritoneum. A second 1–2cm incision was made to open up the peritoneal cavity and a small loop of the intestine was pulled out of the peritoneal cavity. This loop was carefully placed between two coverslips part of a custom made apparatus designed to minimize intestinal contraction during imaging while creating a physiological and comfortable environment for the mouse (McDole et al., 2012). The mouse's normal body temperature was maintained during imaging and continuous oxygenated DMEM high glucose media lacking phenol red (Hyclone) was exchanged over the exposed piece of tissue. Rhodamine B isothiocyanate-dextran (Sigma) was injected i.v. prior to intravital imaging to assess blood flow and the health of the tissue. Movies were acquired using a MP SP5 two-photon microscope TCS (Leica) equipped with a Mai Tai HP DeepSee lasers (SpectraPhysics), an 8,000-Hz resonant scanner, a 25×/0.95 NA objective, two non-descanned detector and two hybrid detectors.

During imaging, continuous oxygenated DMEM high glucose media lacking phenol red (Hyclone) was exchanged in the chamber containing the sample. Tissue was excited at 860 or 890nm and multiple fluorophores were imaged using the custom dichroic mirrors with the following collections: SHG <440nm, CFP 435–485nm, GFP 500–520nm, Hoescht 461nm. Data were processed with Imaris software (version 7.6.4 and version 8.0.1). Migrational analysis were performed using motility lab (created by the MotilityLab team, 2015: Johannes Textor, Jeffrey Berry, Mark J. Miller) or a macro (Fife et al., 2009). The drift correct function in Imaris and motility lab was used to correct SI contraction during imaging where necessary.

For each individual animal, we collected movies of at least two different locations within the jejunum separated by at least 1 mm. Within each of these macroscopic locations, we imaged 3–4 positions concurrently. We removed positions that experienced macro vibrations/ contractions and are usually left with ~3–6 unique positions/animal per a given treatment condition. These individual positions were separately analyzed and averaged to identify typical cell behavior. This was repeated for several mice per condition. For presentation in figures, we showed data from one mouse that most closely approximates the typical cell behavior observed across all mice. Each dot in the motility measurement graphs represents one cell. In the legend, the "n" indicates the number of mice. It can be common for rejection to occur when transferring T cells producing novel fluorochromes (or other antigens) to new hosts for imaging or any other type of analysis for any investigator. We saw no cell behavioral differences between mice with increased attrition of T cells at memory time

points (presumably due to rejection) and mice with normal memory T cell frequencies. In any case, T cells undergoing active rejection/death will be difficult to capture in the process and would likely not be imaged. If expected memory P14 T cell numbers were not detected in blood before analyzing experimental mice, we assumed rejection of memory P14 was occurring and did not use these mice for any analysis, including imaging.

Blocking with antibodies: For K^b-SIINFEKL blocking experiments, mice were i.v. injected with 100μg of anti-K^b-SIINFEKL antibody 1–2 hrs before imaging (25-D1.15, BioXcell). An irrelevant IgG1 antibody was used as an isotype control under the same conditions (MOPC-21, BioXcell).

Mathematical modeling of TPLSM data: For calculating volume, a 360μm by 360μm by 360μm domain was divided into 2.5μm x 2.5μm x 2.5μm cubes. There were 2,985,984 = $(360/2.5)^3$ such cubes. Each cell was initially translated so that its minimum in the x-, y-, and z-directions coincided with the origin (0,0,0). As the cell moved through the domain using observed positions, the distance between the cell and each of the cubes was calculated. An algorithm was used to compute these distances. If the distance between the cell and a cube center was less than a radius of a cell (assumed to be 5μm), then cube volume was counted as part of the total volume traversed by the cell. A specific cube volume is only counted once. The total volume traversed by the cell (μm^3) is divided by the time the cell was observed (in seconds). Straightness analysis was performed as previously described (Mrass et al., 2017). Briefly, for every experimental track, 100 track-derivatives were generated, by randomizing the orientation of individual velocity vectors. The magnitude of the velocity vectors was left unchanged and therefore the average speed was identical in experimental and randomized tracks. The displacement between the start and end of the experimental track and the displacements of 100 randomized tracks were used to calculate the straightness Z-score. It shows how many standard deviations the experimental displacement deviates from the expected displacement of all randomized track derivatives. Negative Z-scores suggest that the experimental displacement is less than expected by chance (“confined tracks”) and positive Z-scores suggest that the experimental displacement is higher than expected by chance (“straight tracks”).

For modeling the length of time expected for P14 CD8 T cells to scan a villus, frequency distributions were created for speed and turning angles using day 30 T cell data within the villi. Simulations were performed using a cylinder with a diameter of 75μm and a height of 300μm, to mimic the shape and size of a single villus in the jejunum. A simulation was performed with 60 cells uniformly distributed within the cylinder (Figure 2A) and with one T cell initially positioned at the center of the cylinder (Figure S2A). T cells sample from the speed and turning angle distributions each time step to advance their position in time. The turning angle determined a cone on which the T cell remained when advancing its position. A time step of 20 seconds was used for the simulation of 60 cells, and a time step of 60 seconds was used for one cell. The cylinder was divided into 85,789 2.5μm by 2.5μm by 2.5μm cubes. A cube was counted towards the total volume patrolled if the distance between a cube center and any T cell was less or equal to the T cell radius (3.5μm). A cube that had been surveyed remained permanently surveyed for the duration of the simulation. If a T cell

attempted to exit the cylinder, it was assigned its previous position with a random 0.5μm displacement component in the x-, y-, and z-direction, such that it remained within the cylinder. The simulations with 60 cells and one cell were repeated 100 times to create error bars. Error bars plot the maximum and minimum volume patrolled over the 100 simulations at a specific time.

QUANTIFICATION AND STATISTICAL ANALYSIS

D'Agostino and Pearson test was performed to evaluate normality. A Mann-Whitney test was performed when two unpaired groups being compared did not exhibit Gaussian distribution. When a single variable between multiple groups with normal distribution was compared, a one-way ANOVA with Dunn's multiple comparison was employed. For single variable comparisons across multiple groups of non-Gaussian distribution, a Kruskal-Wallis test was used. All statistics were performed using Prism (GraphPad Software, V7) and for all analysis p values of less than 0.05 were considered significant, as indicated by one or more asterisks (*).

Supplementary Material

Refer to Web version on PubMed Central for supplementary material.

Acknowledgements

We would like to thank Dr. J. Michael Stolley for schematic artistry; Drs. Yoji Shimizu and Brandon Burbach for providing OT-I-GFP mice and Drs. Stephen Jameson, Kris Hogquist and Tessa Bergsbaken for sharing Kaede transgenic mice and Yptb-OVA. This work was funded by a University of Minnesota Academic Health Center Seed Grant (V.V.) and NIH grant T32AI007313 (E.A.T.) and the University of Minnesota Doctoral Dissertation Fellowship (E.A.T.). B.T.F. and J.S.M. are supported by NIH R01 AI106791. D.T. was supported by UTEP BUILDing SCHOLARS NIH award RL5GM118969.

References

Bergsbaken T and Bevan MJ (2015), "Proinflammatory microenvironments within the intestine regulate the differentiation of tissue-resident CD8$^+$ T cells responding to infection", Nature Immunology, Vol. 16 No. 4, pp. 406–414. [PubMed: 25706747]

Bergsbaken T, Bevan MJ and Fink PJ (2017), "Local Inflammatory Cues Regulate Differentiation and Persistence of CD8(+) Tissue-Resident Memory T Cells", Cell Reports, Vol. 19 No. 1, pp. 114–124. [PubMed: 28380351]

Beura LK, Anderson KG, Schenkel JM, Locquiao JJ, Fraser KA, Vezys V, Pepper M, et al. (2015), "Lymphocytic choriomeningitis virus persistence promotes effector-like memory differentiation and enhances mucosal T cell distribution", Journal of Leukocyte Biology, Vol. 97 No. 2, pp. 217–225. [PubMed: 25395301]

Beura LK, Mitchell JS, Thompson EA, Schenkel JM, Mohammed J, Wijeyesinghe S, Fonseca R, et al. (2018), "Intravital mucosal imaging of CD8 + resident memory T cells shows tissue-autonomous recall responses that amplify secondary memory", Nature Immunology, Vol. 19 No. 2, pp. 173–182. [PubMed: 29311694]

Boissonnas A, Fetler L, Zeelenberg IS, Hugues S and Amigorena S (2007), "In vivo imaging of cytotoxic T cell infiltration and elimination of a solid tumor", The Journal of Experimental Medicine, Vol. 204 No. 2, pp. 345–356. [PubMed: 17261634]

Breart B, Lemaître F, Celli S and Bousso P (2008), "Two-photon imaging of intratumoral CD8$^+$ T cell cytotoxic activity during adoptive T cell therapy in mice", The Journal of Clinical Investigation, Vol. 118 No. 4, pp. 1390–1397. [PubMed: 18357341]

Cahalan MD and Parker I (2008), “Choreography of cell motility and interaction dynamics imaged by two-photon microscopy in lymphoid organs”, Annual Review of Immunology, Vol. 26, pp. 585–626.

Casey KA, Fraser KA, Schenkel JM, Moran A, Abt MC, Beura LK, Lucas PJ, et al. (2012), “Antigen-independent differentiation and maintenance of effector-like resident memory T cells in tissues”, Journal of Immunology (Baltimore, Md.: 1950), Vol. 188 No. 10, pp. 4866–4875.

Celli S, Albert ML and Bousso P (2011), “Visualizing the innate and adaptive immune responses underlying allograft rejection by two-photon microscopy”, Nature Medicine, Vol. 17 No. 6, pp. 744–749.

Chistiakov DA, Bobryshev YV, Kozarov E, Sobenin IA and Orekhov AN (2015), “Intestinal mucosal tolerance and impact of gut microbiota to mucosal tolerance”, Frontiers in Microbiology, Vol. 5, available at:10.3389/fmicb.2014.00781.

Cieza RJ, Cao AT, Cong Y and Torres AG (2012), “Immunomodulation for gastrointestinal infections”, Expert Review of Anti-Infective Therapy, Vol. 10 No. 3, pp. 391–400. [PubMed: 22397571]

Dustin ML, Bromley SK, Kan Z, Peterson DA and Unanue ER (1997), “Antigen receptor engagement delivers a stop signal to migrating T lymphocytes”, Proceedings of the National Academy of Sciences of the United States of America, Vol. 94 No. 8, pp. 3909–3913. [PubMed: 9108078]

Edelblum KL, Shen L, Weber CR, Marchiando AM, Clay BS, Wang Y, Prinz I, et al. (2012), “Dynamic migration of γδ intraepithelial lymphocytes requires occludin”, Proceedings of the National Academy of Sciences, Vol. 109 No. 18, pp. 7097–7102.

Fernandez-Ruiz D, Ng WY, Holz LE, Ma JZ, Zaid A, Wong YC, Lau LS, et al. (2016), “Liver-Resident Memory CD8 + T Cells Form a Front-Line Defense against Malaria Liver-Stage Infection”, Immunity, Vol. 45 No. 4, pp. 889–902. [PubMed: 27692609]

Fife BT, Pauken KE, Eagar TN, Obu T, Wu J, Tang Q, Azuma M, et al. (2009), “Interactions between PD-1 and PD-L1 promote tolerance by blocking the TCR-induced stop signal”, Nature Immunology, Vol. 10 No. 11, pp. 1185–1192. [PubMed: 19783989]

Germain RN, Robey EA and Cahalan MD (2012), “A decade of imaging cellular motility and interaction dynamics in the immune system”, Science (New York, N.Y.), Vol. 336 No. 6089, pp. 1676–1681.

Hallmann R, Zhang X, Di Russo J, Li L, Song J, Hannocks M-J and Sorokin L (2015), “The regulation of immune cell trafficking by the extracellular matrix”, Current Opinion in Cell Biology, Vol. 36, pp. 54–61. [PubMed: 26189064]

Hoytema van Konijnenburg DP, Reis BS, Pedicord VA, Farache J, Victora GD and Mucida D (2017), “Intestinal Epithelial and Intraepithelial T Cell Crosstalk Mediates a Dynamic Response to Infection”, Cell, available at:10.1016/j.cell.2017.08.046.

Konjar Š, Ferreira C, Blankenhaus B and Veldhoen M (2017), “Intestinal Barrier Interactions with Specialized CD8 T Cells”, Frontiers in Immunology, Vol. 8, p. 1281. [PubMed: 29075263]

McDole JR, Wheeler LW, McDonald KG, Wang B, Konjufca V, Knoop KA, Newberry RD, et al. (2012), “Goblet cells deliver luminal antigen to CD103+ DCs in the small intestine”, Nature, Vol. 483 No. 7389, pp. 345–349. [PubMed: 22422267]

McNamara HA, Cai Y, Wagle MV, Sontani Y, Roots CM, Miosge LA, O’Connor JH, et al. (2017), “Up-regulation of LFA-1 allows liver-resident memory T cells to patrol and remain in the hepatic sinusoids”, Science Immunology, Vol. 2 No. 9, p. eaaj1996.

Mowat AM and Agace WW (2014), “Regional specialization within the intestinal immune system”, Nature Reviews. Immunology, Vol. 14 No. 10, pp. 667–685.

Mrass P, Oruganti SR, Fricke GM, Tafoya J, Byrum JR, Yang L, Hamilton SL, et al. (2017), “ROCK regulates the intermittent mode of interstitial T cell migration in inflamed lungs”, Nature Communications, Vol. 8, available at:10.1038/s41467-017-01032-2.

Mrass P, Takano H, Ng LG, Daxini S, Lasaro MO, Iparraguirre A, Cavanagh LL, et al. (2006), “Random migration precedes stable target cell interactions of tumor-infiltrating T cells”, The Journal of Experimental Medicine, Vol. 203 No. 12, pp. 2749–2761. [PubMed: 17116735]

Mueller SN, Hosiawa-Meagher KA, Konieczny BT, Sullivan BM, Bachmann MF, Locksley RM, Ahmed R, et al. (2007), “Regulation of Homeostatic Chemokine Expression and Cell Trafficking During Immune Responses”, Science, Vol. 317 No. 5838, pp. 670–674. [PubMed: 17673664]

Mueller SN, Matloubian M, Clemens DM, Sharpe AH, Freeman GJ, Gangappa S, Larsen CP, et al. (2007), "Viral targeting of fibroblastic reticular cells contributes to immunosuppression and persistence during chronic infection", Proceedings of the National Academy of Sciences of the United States of America, Vol. 104 No. 39, pp. 15430–15435. [PubMed: 17878315]

Müller S, Bühler-Jungo M and Mueller C (2000), "Intestinal intraepithelial lymphocytes exert potent protective cytotoxic activity during an acute virus infection", Journal of Immunology (Baltimore, Md.: 1950), Vol. 164 No. 4, pp. 1986–1994.

Overstreet MG, Gaylo A, Angermann B, Hughson A, Hyun Y, Lambert K, Acharya M, et al. (2013), "Inflammation-induced effector CD4+ T cell interstitial migration is alpha-v integrin dependent", Nature Immunology, Vol. 14 No. 9, pp. 949–958. [PubMed: 23933892]

Pauken KE, Nelson CE, Martinov T, Spanier JA, Heffernan JR, Sahli NL, Quarnstrom CF, et al. (2015), "Cutting edge: identification of autoreactive CD4+ and CD8+ T cell subsets resistant to PD-1 pathway blockade", Journal of Immunology (Baltimore, Md.: 1950), Vol. 194 No. 8, pp. 3551–3555.

Santamaria Babi LF, Moser R, Perez Soler MT, Picker LJ, Blaser K and Hauser C (1995), "Migration of skin-homing T cells across cytokine-activated human endothelial cell layers involves interaction of the cutaneous lymphocyte-associated antigen (CLA), the very late antigen-4 (VLA-4), and the lymphocyte function-associated antigen-1 (LFA-1)", Journal of Immunology (Baltimore, Md.: 1950), Vol. 154 No. 4, pp. 1543–1550.

Schenkel JM, Fraser KA, Vezys V and Masopust D (2013), "Sensing and alarm function of resident memory $CD8^+$ T cells", Nature Immunology, Vol. 14 No. 5, pp. 509–513. [PubMed: 23542740]

Sorokin L (2010), "The impact of the extracellular matrix on inflammation", Nature Reviews Immunology, Vol. 10 No. 10, pp. 712–723.

Steinert EM, Schenkel JM, Fraser KA, Beura LK, Manlove LS, Igyártó BZ, Southern PJ, et al. (2015), "Quantifying Memory CD8 T Cells Reveals Regionalization of Immunosurveillance", Cell, Vol. 161 No. 4, pp. 737–749. [PubMed: 25957682]

Sujino T, London M, Hoytema van Konijnenburg DP, Rendon T, Buch T, Silva HM, Lafaille JJ, et al. (2016), "Tissue adaptation of regulatory and intraepithelial $CD4^+$ T cells controls gut inflammation", Science (New York, N.Y.), Vol. 352 No. 6293, pp. 1581–1586.

Sumida H, Lu E, Chen H, Yang Q, Mackie K and Cyster JG (2017), "GPR55 regulates intraepithelial lymphocyte migration dynamics and susceptibility to intestinal damage", Science Immunology, Vol. 2 No. 18, p. eaao1135.

Thompson EA, Beura LK, Nelson CE, Anderson KG and Vezys V (2016), "Shortened Intervals during Heterologous Boosting Preserve Memory CD8 T Cell Function but Compromise Longevity", Journal of Immunology (Baltimore, Md.: 1950), Vol. 196 No. 7, pp. 3054–3063.

Tomura M, Yoshida N, Tanaka J, Karasawa S, Miwa Y, Miyawaki A and Kanagawa O (2008), "Monitoring cellular movement in vivo with photoconvertible fluorescence protein 'Kaede' transgenic mice", Proceedings of the National Academy of Sciences, Vol. 105 No. 31, pp. 10871–10876.

Vezys V, Olson S and Lefrançois L (2000), "Expression of Intestine-Specific Antigen Reveals Novel Pathways of CD8 T Cell Tolerance Induction", Immunity, Vol. 12 No. 5, pp. 505–514. [PubMed: 10843383]

Wang X, Sumida H and Cyster JG (2014), "GPR18 is required for a normal CD8αα intestinal intraepithelial lymphocyte compartment", The Journal of Experimental Medicine, Vol. 211 No. 12, pp. 2351–2359. [PubMed: 25348153]

Wright NA, Carter J and Irwin M (1989), "The measurement of villus cell population size in the mouse small intestine in normal and abnormal states: a comparison of absolute measurements with morphometric estimators in sectioned immersion-fixed material", Cell and Tissue Kinetics, Vol. 22 No. 6, pp. 425–450. [PubMed: 2611855]

Xu C, Shen Y, Littman DR, Dustin ML and Velázquez P (2012), "Visualization of mucosal homeostasis via single- and multiphoton intravital fluorescence microscopy", Journal of Leukocyte Biology, Vol. 92 No. 3, pp. 413–419. [PubMed: 22457365]

Zaid A, Mackay LK, Rahimpour A, Braun A, Veldhoen M, Carbone FR, Manton JH, et al. (2014), "Persistence of skin-resident memory T cells within an epidermal niche", Proceedings of the National Academy of Sciences, Vol. 111 No. 14, pp. 5307–5312.

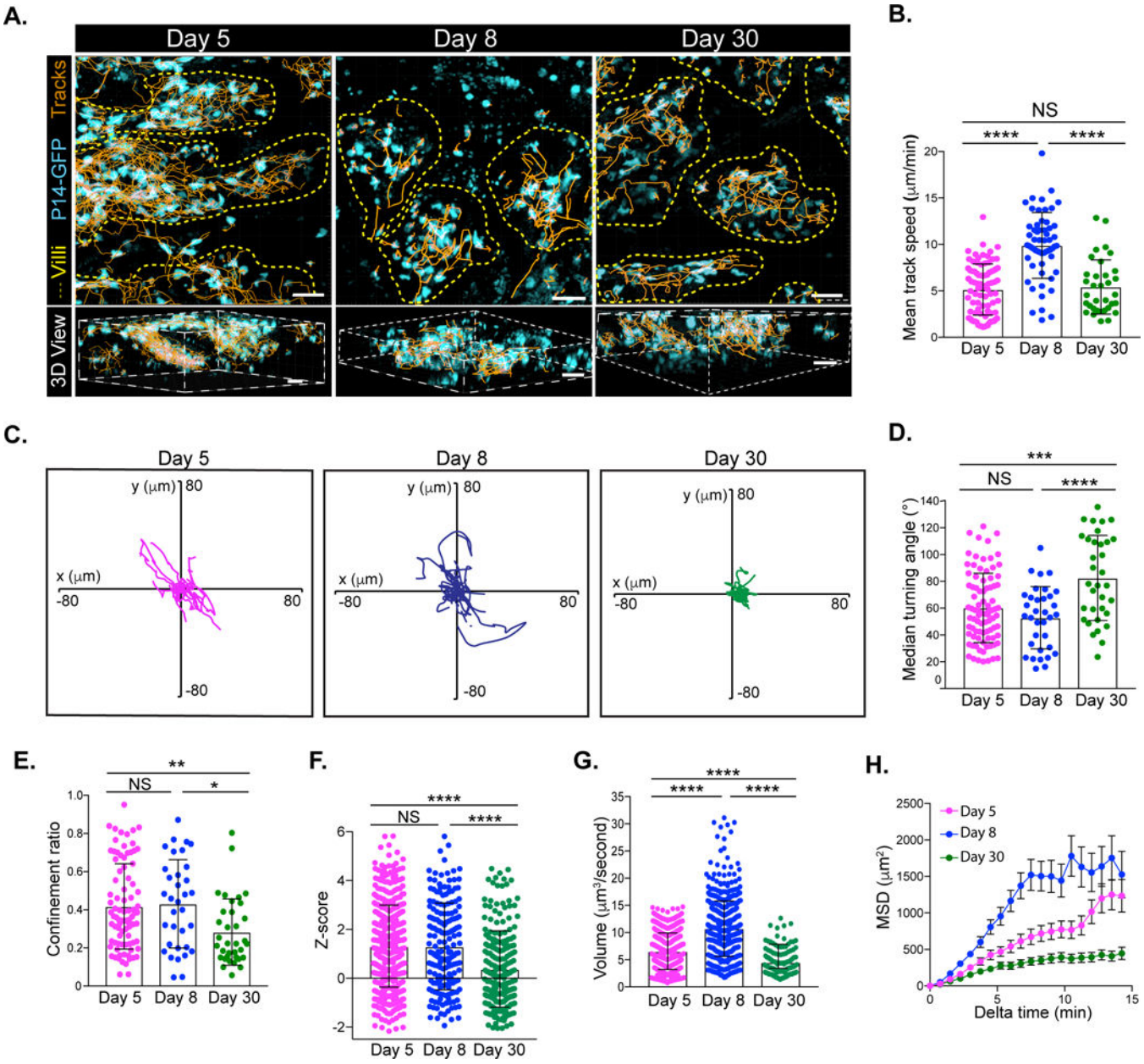

Figure 1). Ag-specific CD8 T cell motility in the small intestine varies during LCMV infection.

Naïve P14-GFP CD8 T cells were transferred to B6 mice and infected with LCMV. **(A)** Cell tracks (orange) of P14-GFP CD8 T cells (cyan) in the villi (outlined in yellow dashed lines) of the jejunum at the indicated time points after LCMV infection in orthogonal (top) or perspective (bottom) presentation. Scale bar is 20μm (top) and 30μm (bottom). **(B)** Mean track speed, **(C)** flower plots of cell track displacements, **(D)** median turning angle, **(E)** confinement ratio, **(F)** Z-straightness, **(G)** volume scanned and **(H)** mean squared displacement (MSD) as a function of time of P14-GFP CD8 T cells in the villi at days 5 (magenta), 8 (blue), and 30 (green) after LCMV infection. Dots in motility graphs represent individual cells imaged. Data of motility parameters presented in bar graphs are derived from the same mouse at the time point indicated. Data are representative of 2 or more

experiments with mice totaling n=4 for day 5, n=7 for day 8, and n=8 for day 30. A one-way ANOVA with Dunn's multiple comparison test was performed to evaluate statistical significance. ****p=<0.0001, ***p=<0.0003, **p=0.006, and *p=0.01. All error bars are SD. See also Figure S1.

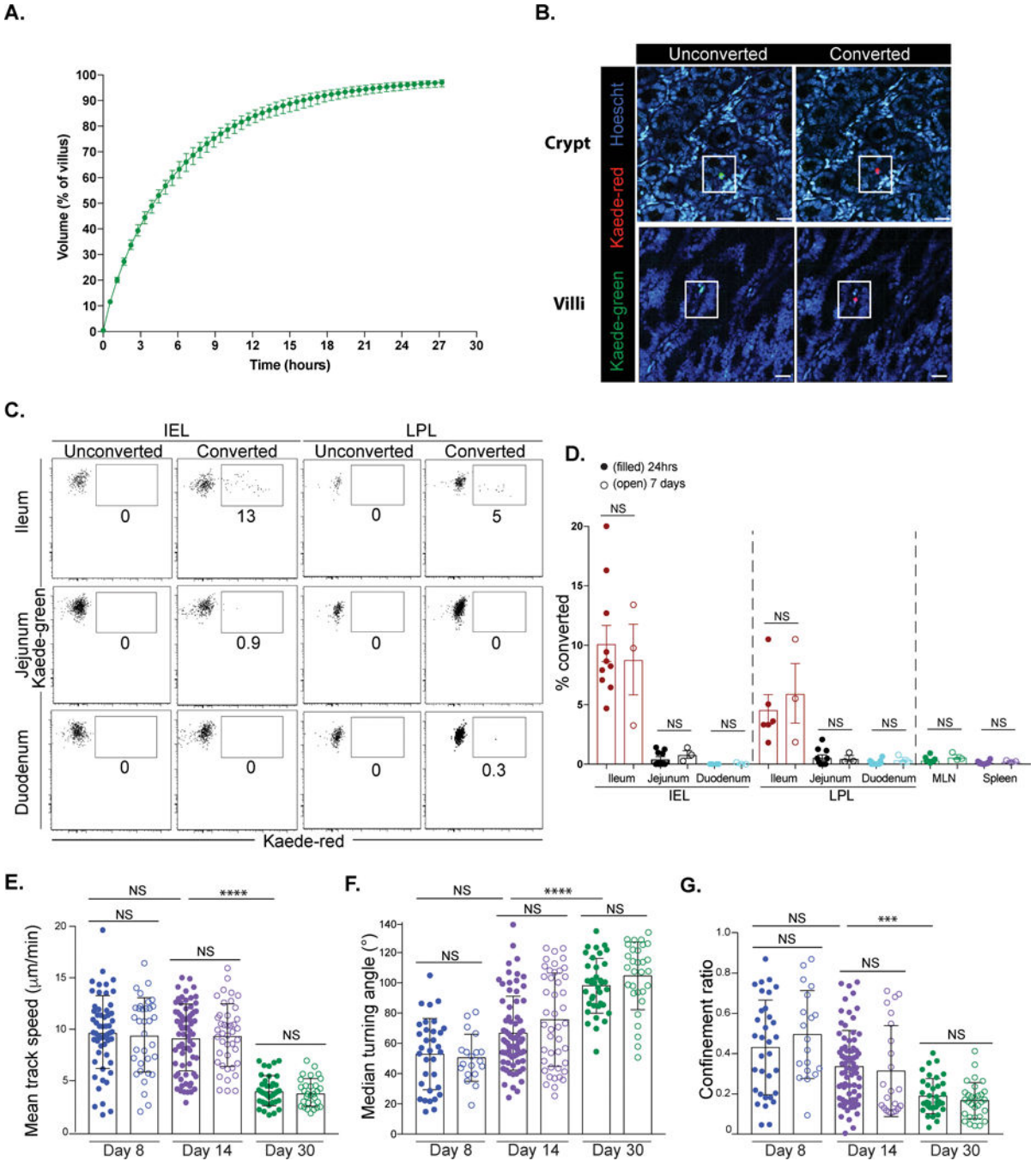

Figure 2). CD8 T_{RM} have restricted locomotion in the small intestine.

(A) Modeling of 60 P14 CD8 T_{RM} scanning a single villus. Data shown are the time taken to scan the indicated portion of the villus by 60 P14. Error bars show the maximum and minimum volume patrolled over 100 simulations at a specific time. **(B-D)** A section of the ileum of OT-I/Kaede memory mice was exposed to 405nm light. One or 7 days later, portions of the SI were evaluated for converted OT-I/Kaede cells. **(B)** Unconverted (green) or converted (red) OT-I/Kaede T cells were visualized in the SI +/− light exposure. Scale bar is 20μm. **(C)** Flow cytometric analysis of OT-I/Kaede IEL and LPL in the indicated sections of

the intestine 24 hours after conversion. Plots are gated on OT-I CD8 T cells. Sham surgery mice were used as unconverted controls. **(D)** Frequency of photoconverted cells (Kaede-red) in indicated locations 24 hours (filled) and day 7 (open) after conversion. A Mann-Whitney test was used to evaluate significance. Data are representative of three experiments, n=10 mice. Error bars are SEM. **(E-G)** Naïve P14-GFP and P14/CD103$^{-/-}$-CFP CD8 T cells were transferred to B6 mice and infected with LCMV. **(E)** Mean track speed, **(F)** median turning angle and **(G)** confinement ratio of P14-GFP and P14-CFP CD8 T cells at day 8 (blue), day 14 (purple) and day 30 (green). Filled circles=WT P14-GFP; open circles= P14/CD103$^{-/-}$-CFP. Dots in motility graphs represent individual cells imaged. Data of motility parameters presented in bar graphs are derived from the same mouse at the time point indicated. Data are representative of 2 experiments with mice totaling n=5 for day 8, n=5 for day 14 and n=4 for day 30. A Kruskal-Wallis one-way ANOVA with Dunn's multiple comparison test was performed to evaluate statistical significance. ****p=<0.0001 and ***p=0.007. Error bars are SD. See also Figures S2–3.

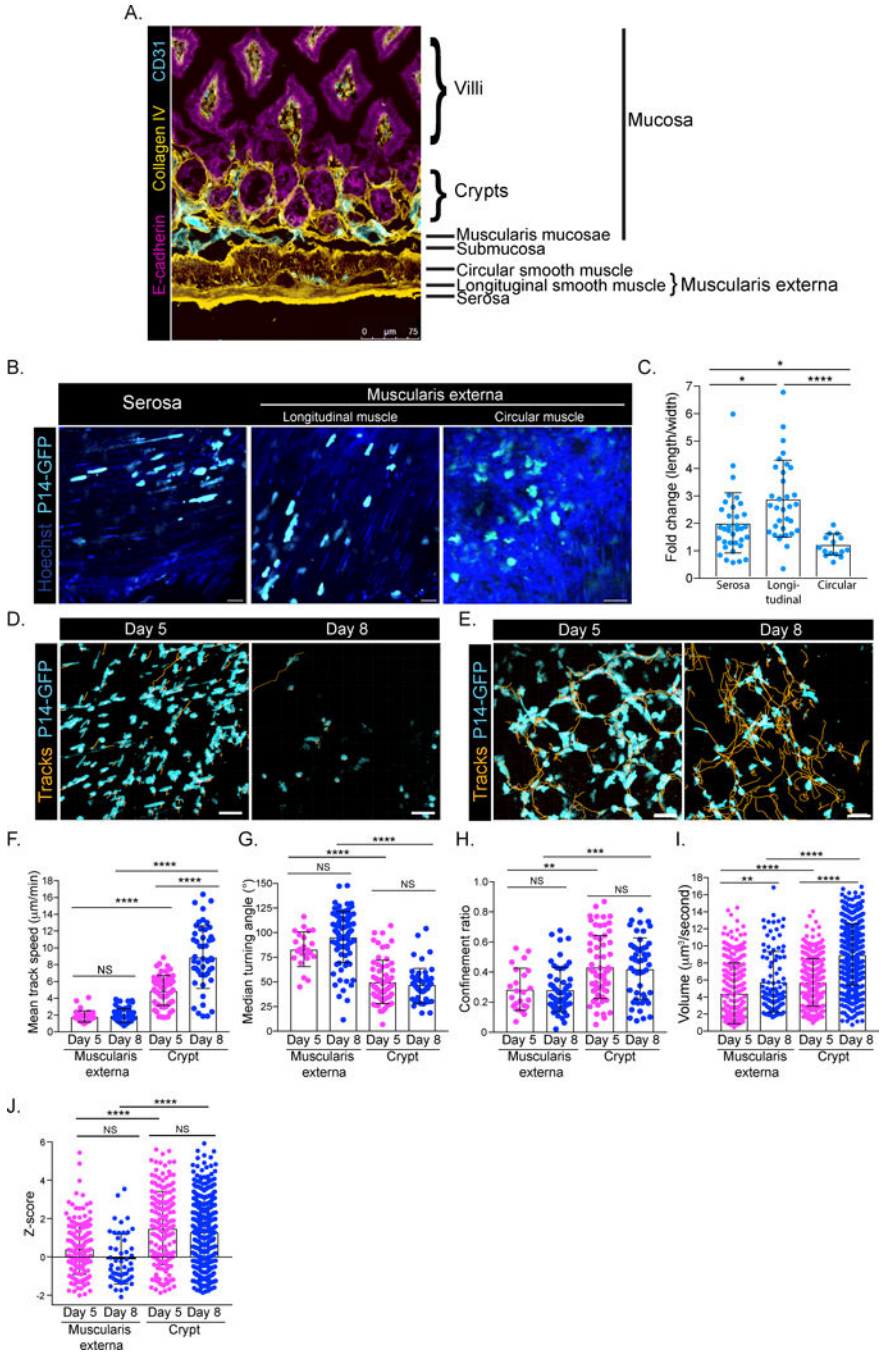

Figure 3). Tissue architecture dictates CD8 T cell motility in the small intestine.

(A) Histological section of SI jejunum stained with E-cadherin (magenta), collagen IV (yellow) and CD31 (cyan). Scale bar is 75μm. **(B)** P14-GFP CD8 T cells were transferred to B6 and infected with LCMV. Five days post infection, P14-GFP CD8 T cells (cyan) in the serosa and muscularis externa were imaged using TPLSM. Hoechst stain (dark blue) was injected prior to imaging. **(C)** Fold change of length/width measurements of individual P14-GFP CD8 T cells in the serosa, longitudinal muscle and circular muscle at day 5 after LCMV. **(D)** Cell tracks (orange) of P14-GFP CD8 T cells (cyan) in the muscularis externa

and serosa at days 5 and 8 after LCMV infection. **(E)** Same as in D, but in crypts of SI. Scale bars in B, D, E are 20μm. **(F)** Mean track speed, **(G)** median turning angle, **(H)** confinement ratio, **(I)** volume scanned and **(J)** *Z*-score of P14-GFP CD8 T cells at days 5 (magenta) and 8 (blue) after LCMV infection in the indicated locations of the SI. Dots in motility graphs represent individual cells imaged. Data of motility parameters for each specific experiment presented in bar graphs are derived from the same mouse at the time point indicated. Data are representative of at least 2 experiments with mice totaling n=4 for day 5 and n=5 for day 8 in the muscularis externa and n=5 for day 5 and n=7 for day 8 in the crypt. A Kruskal-Wallis one-way ANOVA with Dunn's multiple comparison test was performed to evaluate statistical significance. ****p=<0.0001, ***p=0.0003 **p=<0.003 and *p=<0.05. All error bars are SD.

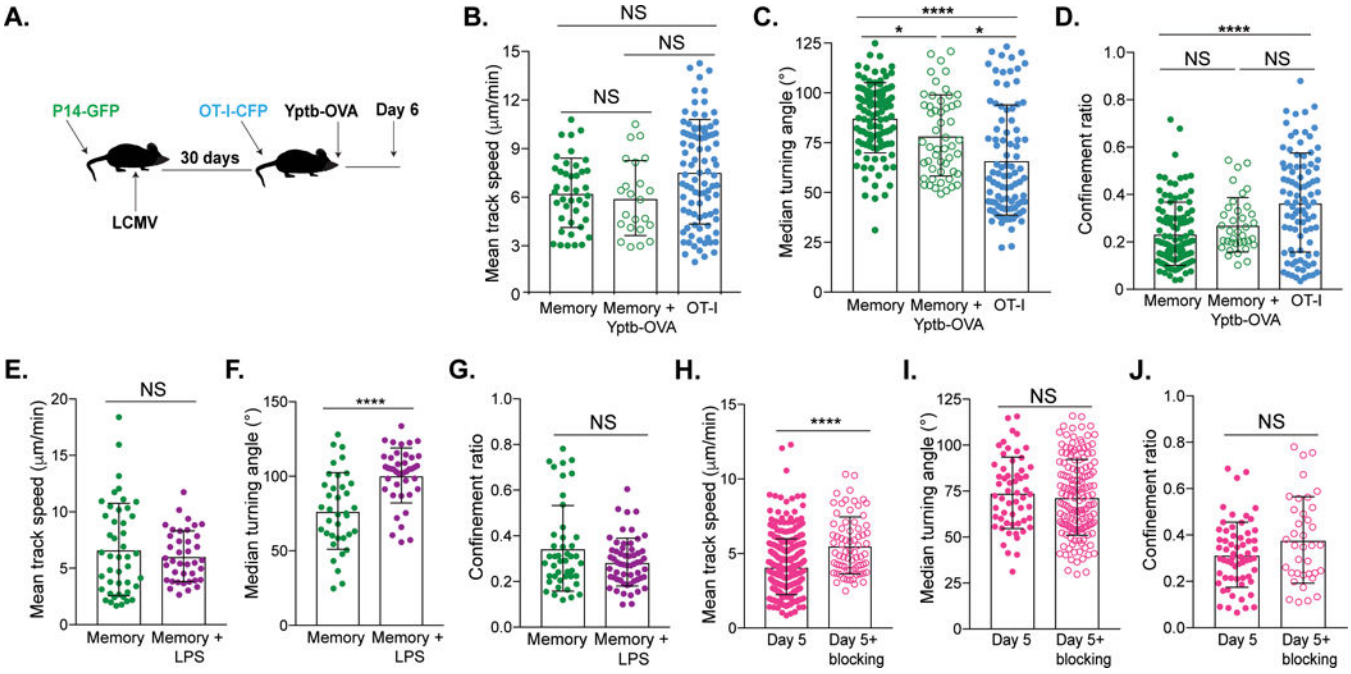

Figure 4). Bystander inflammation impacts CD8 T_{RM} motility.

(A-D) Memory P14-GFP mice received OT-I-CFP CD8 T cells and were orally infected with Yptb-OVA 1 day later. Cells were imaged in the jejunum 6 days later. **(A)** Experimental setup. **(B)** Mean track speed, **(C)** median turning angle and **(D)** confinement ratio of memory P14-GFP CD8 T during Yptb-OVA infection (green, open) and day 6 OT-I-CFP CD8 T cells (blue, filled), compared to steady state P14-GFP memory CD8 T cells (green, filled). Data are representative of at least 2 experiments totaling n=4 mice for experiments with Yptb-OVA and n=4 mice for experiments with memory at steady state. A Kruskal-Wallis one-way ANOVA with Dunn's multiple comparison test was performed to evaluate statistical significance. ****p=<0.0001, ***p=0.0002. **(E-G)** Memory P14-GFP mice were injected intraperitoneally with 4mg/kg LPS and imaged 4–5 hours later. **(E)** Mean track speed, **(F)** turning angle and **(G)** confinement ratio of P14-GFP CD8 T cells in the absence (green) or presence (purple) of LPS. Experiments are representative of n=4 memory+LPS mice and n=2 memory mice. Mann-Whitney tests were used to evaluate significance. ****p=<0.0001. **(H-J)** OT-I-GFP CD8 T cells were transferred to iFABP-OVA mice and evaluated 5 days after transfer +/− K^b-SIINFEKL blocking antibody. **(H)** Mean track speed, **(I)** median turning angle and **(J)** confinement ratio of day 5 (magenta, filled) and day 5+blocking Ab (magenta, open) OT-I-GFP CD8 T cells. Data represent at least 2 experiments, n=3 mice without blocking and n=3 mice with blocking. Mann-Whitney tests were performed to evaluate statistical significance. ****p=<0.0001. All error bars are SD. In all graphs measuring motility, dots represent individual cells imaged. Data of motility parameters for each specific experiment presented in bar graphs are derived from the same mouse at the time point indicated. See also Figure S4.